ACS APPLIED MATERIALS & INTERFACES

RESEARCH ARTICLE

www.acsami.org

Linear/Network Poly(ε-caprolactone) Blends Exhibiting Shape Memory Assisted Self-Healing (SMASH)

Erika D. Rodriguez,[†,§] Xiaofan Luo,[‡,§] and Patrick T. Mather*[,‡,§]

[†]Mechanical and Aerospace Engineering, [‡]Biomedical and Chemical Engineering, and [§]Syracuse Biomaterials Institute, Syracuse University, New York 13244, United States

Supporting Information

ABSTRACT: Self-healing (SH) polymers are responsive polymeric materials that can repair mechanical damage such as cracks in an autonomous fashion. In most SH polymers studies reported to date, crack closure was either unaddressed or achieved by manual intervention. Here, we report a new strategy that utilizes shape memory (SM) to prepare novel SH polymers that are capable of simultaneously closing and rebonding cracks with a simple thermal trigger. This strategy, termed "shape memory assisted self-healing (SMASH)", is demonstrated in a blend system consisting of cross-linked poly(ε-caprolactone) network (n-PCL) with linear poly(ε-caprolactone) (l-PCL) interpenetrating the network, and exhibits a combination of SM response from the network component and SH capacity from the linear component. Thermomechanical analysis revealed that the thermoset, n-PCL, demonstrates reversible plasticity —a form of shape memory where large plastic deformation at room temperature is fully recoverable upon heating. This SM action assists to close any cracks formed during deformation and/or damage while l-PCL chains tackify the crack surfaces by diffusion to the free surface and ultimately across the area of damage during the same heating step as used for SM. In our study, we investigated the controlled damage and SMASH healing of blends with varying composition using tensile testing of essential work of fracture film specimens. The healing component, l-PCL used had a high M_w (M_w ~65k g/mol) to enable re-entanglement after diffusion across the interface while the shape memory component, n-PCL was prepared from PCL telechelic diacrylates and a tetrathiol cross-linker, yielding excellent shape memory. We found excellent self-healing of films by the SMASH mechanism, with near complete healing for l-PCL contents exceeding 25 wt %. Applications are envisioned in the area of self-healing bladders, inflated structure membranes, and architectural building envelopes.

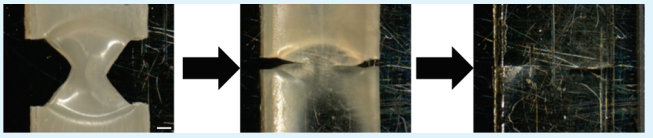

KEYWORDS: shape memory, self-healing, SMASH, reversible plasticity

INTRODUCTION

The shape memory effect in polymers is a phenomenon wherein the polymeric article can be deformed to a temporary shape and stored in that form until later being triggered to return to its original state when stimulated by external heating or other means.[1−4] Such materials are considered enabling for a large number of applications in such diverse industries as automotive, architecture, aerospace, and medical devices. For semicrystalline networks (type II SMPs as defined by Liu et al.,[5] also the current case as will be detailed later), a temporary deformation can be fixed by the crystallization of polymer chains when cooling below T_m[4,6] and the permanent shape may be recovered when the sample is heated above T_m because of the presence of permanent/covalent cross-links, under the action of rubber elasticity. In particular, the cross-links serve as permanent anchors for the network chains to return to their state of highest conformational entropy.[3] In our case, the cross-links were formed when the functional ends (acrylate) of network chain macromers reacted with thiol groups of a multifunctional cross-linker molecule using thiol−ene chemistry.[7−10] Previous studies have successfully used similar systems to create polymer materials with SM properties.[1,2,6,7]

Cracks that form in the bulk of a polymeric material caused by thermal, mechanical, chemical, and/or UV radiation stimulation are hard to detect and thus repair.[11] This damage has become a problem as the material's mechanical properties are severely compromised.[12] In fact, SH was a concept developed in the 1980s as a way to heal cracks that were not externally visible, in order to prolong the life of polymeric materials.[11] SH is a mechanism where microcracks rebond to heal the area of damage. One example of accomplishing SH is through macromolecular chain interdiffusion where the SH is triggered when the material is exposed to above its T_m, a common method of healing among thermoplastic semicrystalline polymers.[11] Other SH systems incorporate microencapsulated healing agents where a propagated crack will rupture the capsule allowing the agent to fill in the damaged site by capillary action and bond the crack surfaces via in situ polymerization.[12−14] For example, White et al. have demonstrated an autonomous healing polymeric composite system which integrates a ruthenium-based Grubbs' catalyst that initiates ring-opening metathesis polymerization of dicyclopentadiene (DCPD) in a thermoset matrix.[12] Because of damage, a crack will form in the bulk of the material, rupturing a monomer-filled microcapsule and lead to flow of the monomer into the crack site by capillary action. The Grubb's

Received: August 11, 2010
Accepted: December 28, 2010
Published: January 21, 2011

catalyst particles, which are randomly distributed throughout the matrix, will trigger polymerization upon contact with the monomer (here, the healing agent), even at room temperature, causing rebonding of the crack surfaces.[12]

As another capsule-based SH approach, the same group has reported on a self-healing poly(dimethyl siloxane) (PDMS) elastomer wherein two types of microcapsules are distributed within the matrix: (i) resin microcapsules that contains high-molecular weight, vinyl-functionalized PDMS and platinum catalyst, and (ii) microcapsules containing hydride-functionalized PDMS for reaction with the vinyl-functionalized resin of (i) in the presence of the platinum catalyst.[15] This material showed good SH response for films whose tears where realigned externally. Even solvents have been used as healing agents for thermosets. For example, solvent-containing microcapsules of phenylacetate (PA) and ethyl phenylacetate (EPA) have been dispersed in the EPON 828 epoxy system for SH purposes.[16] In this system, rupture of the capsules releases the solvent, locally swelling the epoxy matrix, yielding chain mobility, residual monomer diffusion, and rebonding. Such action allows for additional, localized cross-linking and associated healing of the damaged areas.[16] Other work has included functional repair components that are in hollow glass fibers (HGF) and embedded in either carbon-fiber-reinforced epoxy or glass-fiber-reinforced epoxy in order to alleviate damage and sustain mechanical strength.[17−19] These systems are different from microencapsulated polymeric systems as the HGF serves to store functional agents for self-repairing composites while also serving to reinforce the entire system.[18]

The SH systems described above all rely solely on a rebonding reaction, but do not provide often needed crack closure before healing. Addressing this need, Kirkby et al.[20,21] ingeniously integrated both SM and SH in a single material system. In their first report,[20] a small number of pretensioned shape memory alloy (SMA) wires were placed perpendicular to the crack surfaces of a tapered dual cantilever beam (TDCB) specimen made of a diethylenetriamine (DETA) cured epoxy resin, EPON 828 with Grubb's catalyst embedded in the resin matrix for later healing. "Self-healing" was conducted by manually injecting DCPD monomers to the crack and activating the recovery (contraction) of SMA wires by passing through an electrical current, which led to significant crack closure (reduction of crack surface separation) and improved healing. The same strategy was later adopted in a microcapsule-based system[21] to achieve autonomous self-healing. Although proven to be effective in obtaining better healing under controlled laboratory conditions, this SMA-based approach presents several drawbacks for practical applications. First, the SMA wires provide only a unidirectional recovery force; this means they have to be placed perpendicular to the crack in order to be effective. This is hard to realize because, unlike TDCB specimens, the directions of crack propagation in real applications are hardly predictable. Second, the incorporation of SMA wires leads to increased material cost and processing complexity. Therefore, better strategies to achieve crack closure in SH polymers are still needed. This has been the main motivation of the current contribution. Other SH systems have been reported for which a combination of thermosetting resin and thermoplastic was used. Hayes et al.[22] studied epoxy resins (LY1556 and GY298), which served as the thermosetting host matrices, and linear poly(bisphenol A-co-epichlorohydrin), which served as a thermoplastic healing agent. This system proved to be a solid-state healable system where the thermoplastic remained dissolved in the matrix upon curing. After the blend was fractured and then heated, the thermoplastic diffused to the damaged site, sealing the crack and healing the damage. In a similar manner, another group reported a blend of triethyltetramine (TETA) cured diglycidyl ether of bisphenol A (DGEBA) resin with polyethylene-co-methacrylic acid (EMAA) being incorporated as the healing agent.[23] It was found that EMAA formed a discrete phase in the resin (unlike the prior system) and reacted with the resin during healing. EMAA also showed an ability to achieve fracture strength recovery without the need of external forces to assist in healing. Our group has reported on a polymerization-induced phase separation (PIPS) system where a diglycidyl ether of bisphenol A (DGEBA) epoxy−resin-polycaprolactone (PCL) blend was used to enable a unique mechanism of self-healing.[24] The miscible blend underwent PIPS during epoxy cross-linking to produce a "brick and mortar" morphology that afforded thermal mending and reversible adhesion through "bleeding" of the PCL component under the action of differential thermal expansion of liquid PCL and solid epoxy. Finally, reversible chemistry has been exploited for self-healing by Bergman and Wudl.[25,26] In their work, covalent bonds broken during damage could be reformed by application of heat, allowing flow, and subsequent cooling that allowed rebonding.

Until now, fully polymeric systems exhibiting both SM and SH mechanisms have yet to be studied and that is the topic of the present contribution. In this paper, we report on a unique system called shape memory assisted self-healing (SMASH), a concept we first introduced in 2009.[27] This system incorporates a covalently cross-linked network by end-linking end-functionalized poly(ε-caprolactone) (n-PCL) as a thermoset for SM properties and a linear poly(ε-caprolactone) (l-PCL) thermoplastic to provide a SH property. (Here, "l" in "l-PCL" stands for "linear".) This SMASH material can achieve reversible plasticity shape memory (RPSM), a novel phenomenon which we define as the recovery of both the temporal elastic and plastic region of deformation. Consequently, gross damage in proximity to the crack(s) from damage can be reversed by heating.[1,5,6,28] The SMASH material incorporates a thermoplastic interpenetrating into the thermoset, pre- and postphotopolymerization. They also have near-identical T_m values, enabling use of a single heating phase to trigger both the SM and SH mechanisms without compromising the mechanical integrity of the entire system. We contend that such a system with fast and complete healing during a single heating event is quite original and capable of enabling easily maintained mechanical systems involving polymeric films under load, such as inflated structures or containment bladders. We prove that the SMASH concept works well without the addition of fiber or wire reinforcements and without external injection of healing agents.

EXPERIMENTAL SECTION

Materials. Poly(ε-caprolactone) diol ($M_n \approx 3000$ g/mol) (Scientific Polymer Products, Inc.) was first vacuum-dried at room temperature (RT) overnight to remove any adsorbed moisture prior to use. Poly(ε-caprolactone) (l-PCL) ($M_w \approx 65\,000$ g/mol), pentaerythritol tetrakis(3-mercaptopropionate) (tetrathiol) 97%, anhydrous benzene (99.8%), triethylamine (99%), acryloyl chloride (98%), 2,2-dimethoxy-2-phenylacetophenone (DMPA) 99%, and deuterated chloroform, (99.8%

Scheme 1. Preparation of the Poly(ε-caprolactone) Diol (3k) Macromer by End-capping of PCL Diol with Acryloyl Chloride

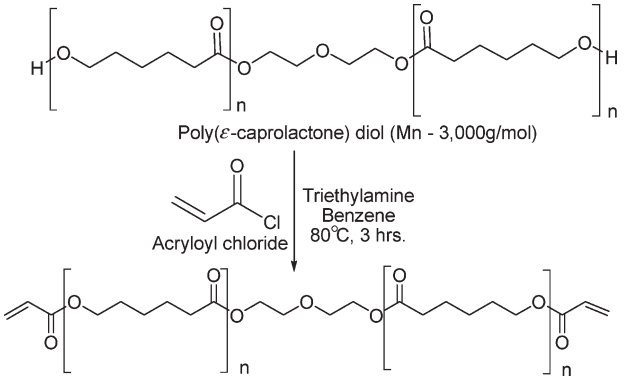

deuteration), all purchased from Sigma Aldrich, and hexane (Fisher Scientific), were used as received.

Poly(ε-caprolactone) Diacrylate Synthesis. Ten grams (3.3 mmol) of poly(ε-caprolactone) (PCL) diol was dissolved in 60 mL of anhydrous benzene under nitrogen purge at RT; 1.184 mL (8.5 mmol) of triethylamine and 0.694 mL (8.6 mmol) of acryloyl chloride was then added dropwise with constant magnetic stirring. The reaction was then carried out at 80 °C for 3 h. The solution was filtered to remove triethylamine hydrochloride and precipitated in 600 mL of hexane to yield a white powder, following which it was dried under vacuum (30 in Hg) at 65 °C overnight (Scheme 1). ^{1}H NMR analysis was then conducted to determine the degree of acrylate end-capping ($CDCl_3$, 4 mg/mL). The acrylate end-capping conversion ratio was calculated from the NMR spectra as described in the Supporting Information and the conversion ratios ranged from 97 to 108% (quantitative conversion, within error) consistent with prior literature using this method.[7] ^{1}H NMR of PCL diacrylate (3k): (a) 4.07 (t, $-CH_2-CH_2-OCO-$), (b+d) 1.65 (m, $-CH_2-CH_2-O$, $-CH_2-CH_2-OCO-$), (c) 1.39 (m, $-CH_2-CH_2-CH_2-$), (e) 2.31 (t, $-OOC-CH_2-CH_2-$), (f) 4.24 (t, $-COO-CH_2-CH_2-O-$), (g) 3.70 (t, $-COO-CH_2-CH_2-O-$), (h) 6.12 (dd, $-OCO-CH=CH_2$), (i) 6.40 (dd, $-OCO-CH=CH_2cis$), (j) 5.83 (dd, $-OCO-CH=CH_2trans$) where the letters a–j correspond to the NMR spectrum shown in Figure S2 in the Supporting Information, where the end-capping conversion values are shown. In preparing formulations for cross-linking, it was assumed that each PCL diacrylate featured a functionality of 2. As we will show, subsequent end-linking by thiol–ene reaction led to high gel fractions (Figure S1 in the Supporting Information shows the NMR spectrum for PCL diol(3k) followed by the repeat unit (n) values needed to calculate the end-capping conversions).

l-PCL:n-PCL Blends. Linear/network blends were prepared by cross-linking of PCL diacrylate with tetrathiol in the presence of linear PCL (Scheme 2). Here, we show the reaction mechanism of thiol–ene addition that dominates over free-radical polymerization at large thiol:ene ratios,[29] though the acrylate end-groups themselves can undergo some competing chain-growth polymerization. The use of a thiol cross-linker for ene-based systems has become prevalent[10,29,30] because of advantages such as oxygen insensitivity and mobility of the thiyl radical.[10] Thus, l-PCL, PCL diacrylate and tetrathiol cross-linker (molar ratio of (PCL diacrylate)/tetrathiol =2:1) of various l-PCL wt % were mixed in 1.2 mL of chloroform (50% w/v) by continuous magnetic stirring at RT until a clear, homogeneous solution was obtained. DMPA (2% relative to PCL diacrylate) was then added and quickly dissolved. The solution was injected to a custom-made glass mold that consisted of two glass slides (75 mm × 25 mm × 1 mm) with a 1 mm thick Teflon spacer placed in between the glass slides. The mixture was exposed to uniform UV irradiation at a power of 60 W, and λ_{max} of 352 nm for 1 h at RT in a custom-made UV curing box consisting of two banks (top and bottom) of UV lamps.[31] The cured samples were removed from the mold and then placed under vacuum (30 in Hg) at 75 °C overnight for complete chloroform removal. The samples are named as l-PCL$_x$:n-PCL$_y$ where x and y stand for the weight percent of l-PCL and PCL diacrylate, respectively. Here, the mass of the cross-linker is excluded in the nomenclature weight percent for simplicity. The following compositions were prepared using the above method (l-PCL$_{wt\ \%}$:n-PCL$_{wt\ \%}$): l-PCL$_0$:n-PCL$_{100}$, l-PCL$_{10}$:n-PCL$_{90}$, l-PCL$_{20}$:n-PCL$_{80}$, l-PCL$_{25}$:n-PCL$_{75}$, l-PCL$_{35}$:n-PCL$_{65}$, l-PCL$_{50}$:n-PCL$_{50}$, l-PCL$_{60}$:n-PCL$_{40}$, l-PCL$_{70}$:n-PCL$_{30}$, l-PCL$_{80}$:n-PCL$_{20}$.

To evaluate the extent of network formation, we conducted gel fraction measurements by first weighing and then immersing a small cured film in 20 mL of chloroform with constant agitation in a shaker (New Brunswick, C24) at 75 rpm and T = 37 °C for 24 h, extracting completely the chloroform-soluble l-PCL, as well as unreacted PCL diacrylate components. After drying under vacuum at 65 °C overnight the sample mass was measured and the gel fraction was calculated according to

$$G(\%) = \frac{m_d}{m_i}100 \quad (1)$$

where m_i is the initial dry weight before extraction and m_d is the dry weight after extraction.[6,12] Gel fraction experiments were conducted for three samples for each composition.

Thermal Characterization. The thermal properties and phase behavior of the l-PCL:n-PCL blends were characterized using thermogravimetric analysis (TGA) and differential scanning calorimetry (DSC), anticipating pertinence to mechanical properties and healing behavior studied later. For the former, each sample with a mass ranging from 3.0 to 5.0 mg was loaded in a TA Q500 TGA instrument. The temperature was then ramped linearly to 600 at 10 °C/min (see Figure S3 in the Supporting Information) under constant nitrogen purge to monitor the decomposition events evidenced by mass changes. DSC experiments were conducted using a TA Q200 DSC instrument equipped with a refrigerated cooling system (RCS). First, the samples were cooled to an equilibration temperature of −85 °C, heated to 120 at 10 °C/min, equilibrated at 120 °C for 1 min, cooled to −90 at 3 °C/min, equilibrated at −90 °C for a 1 min, and finally heated to 120 at 10 °C/min where the first cooling and second heating traces were recorded for detailed study. Three separate experiments were conducted for each composition to ensure reproducibility (see Table S4 in the Supporting Information for T_m, ΔH_m, T_c, and ΔH_c averages).

Dynamic Mechanical and Shape Memory Analyses. Dynamic mechanical and shape memory properties of all compositions were studied using a TA Q800 dynamic mechanical analyzer (DMA). Each sample was cut from a film cross-linked as described above to yield tensile bar specimens with typical dimensions of 5.7 mm (length) × 2.5 mm (width) × 0.7 mm (thickness) and loaded under tension in the DMA apparatus. To measure linear viscoelastic properties and clearly reveal the thermal transitions, an oscillatory tensile deformation was applied with a small displacement amplitude of 15 μm (tensile strain <0.4%), a frequency of 1 Hz, and a "force track" (the ratio of static to dynamic forces) of 110%. The temperature was first ramped to 90 at 3 °C/min to remove the thermal history, held isothermally at 90 °C for 20 min, then cooled down to −90 at 3 °C/min, held isothermally at −90 °C for 5 min, and finally heated to 120 at 3 °C/min. The tensile storage modulus values (E') and tan δ values from the second heating trace are reported. This DMA procedure was tested at least two times for every sample, and confirmed excellent reproducibility.

Scheme 2. Preparation Blends Containing n-PCL and l-PCL by UV-initiated Thiol−ene Polymerization in the Presence of Nonreactive l-PCL

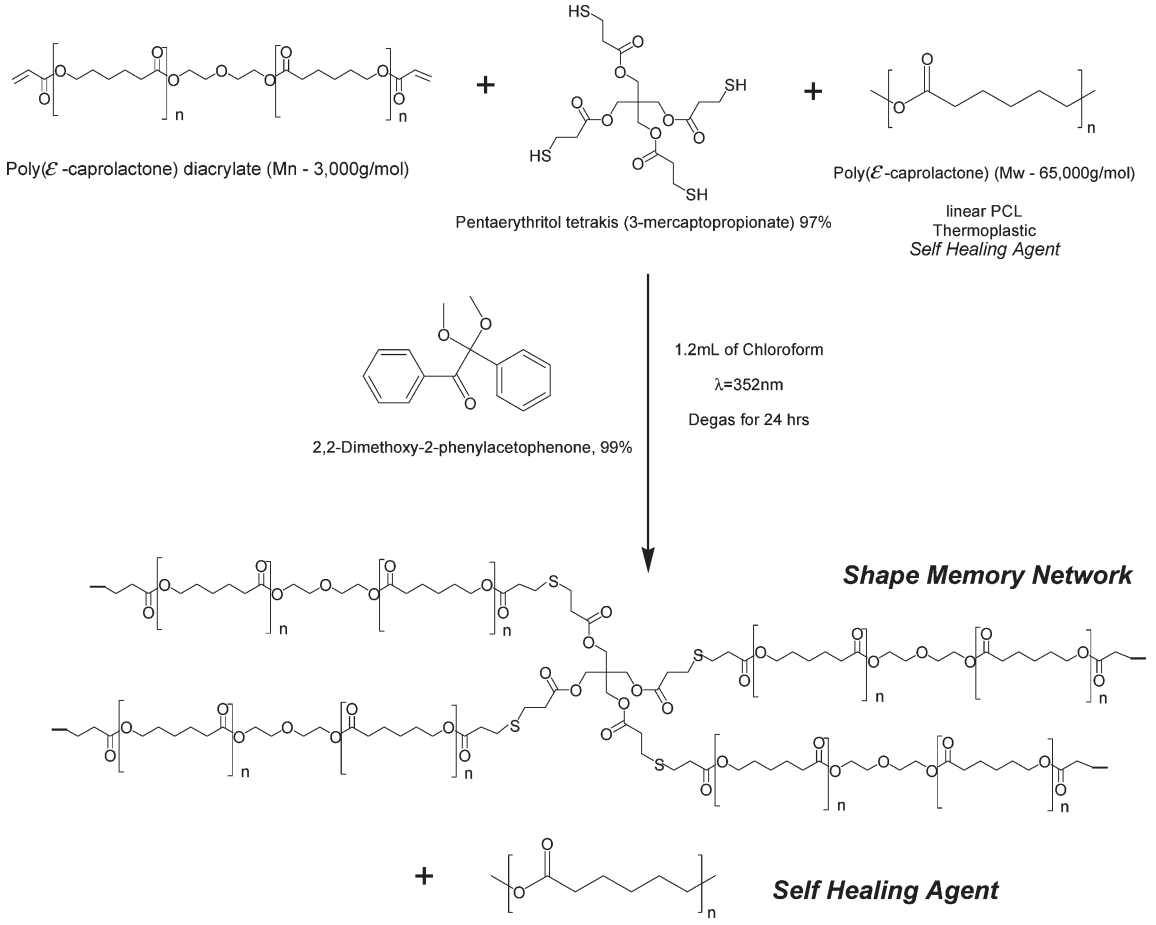

Shape memory of a particular type, reversible plasticity shape memory (RPSM), was examined for all compositions following a modified four-step thermomechanical cycling method,[32] now described. Each sample was punched into a dogbone geometry following the ASTM D638−03 Type V (scaled down by a factor of 2, TestResources, Inc., Shakopee, MN) with an average thickness of 0.5 ± 0.1 mm. Prior to testing, each sample was first placed in a preheated oven (Fisher Scientific Isotemp 825F) at 80 °C (>PCL T_m) for 10 min and left at RT for 10 min to eliminate the effects of thermal history (this will be referred to as thermal mending hereafter). During testing, the sample was first stretched at RT from a preloaded strain (ε_i) to a strain of 200% at a rate of 5%/min and held at 200% strain for 10 min to allow stress relaxation, yielding a strain of ε_m (step 1). To release the force/stress, the strain was programmed to decrease at 5%/min until the force reached a small value of 0.001 N, after which a large percentage of plastic strain/deformation remained (ε_u) for all the samples tested (step 2). Shape recovery was then triggered by heating to 80 at 3 °C/min at this same low load (step 3) to a recovered strain, ε_r. Finally, the temperature was ramped back to 25 at 3 °C/min to complete the SM cycle (step 4). The fixing (R_f) and recovery (R_r) ratios were calculated for each composition. R_f was calculated using $R_f(\%)=(\varepsilon_u/\varepsilon_m) \times 100$ and R_r obtained by using $R_r\,(\%) = (\varepsilon_u - \varepsilon_r)/(\varepsilon_u - \varepsilon_i) \times 100$, where each of the strains are defined above.

Self-Healing Experimentation. Self Healing (SH) experiments were conducted using the deeply double-edge notched tensile (DDEN-T) geometry employed for fracture testing of polymeric films.[31−33] Cured l-PCL:n-PCL blend samples were first cut into a dogbone geometry (ASTM D638−03 Type 1, scaled down by a factor of 3), with an average thickness of 0.56 ± 0.08 mm and a width of 4.3 mm, using a custom-made dogbone cutting die (TestResources, Inc., Shakopee, MN). For such specimens, the gauge length is 16.67 mm. The samples were thermally mended under the same conditions as the recovery step of SM experiments described above. Each sample was loaded in a TST350 Linkam Tensile Stress Testing Stage (Linkam Scientific Instruments, Ltd.) with a 200 N load cell and uniaxially stretched to a displacement of 10 mm (corresponding to a strain of 60% at a displacement rate of 0.1 mm/s (0.6%/s) at RT. After being removed from the stage, the sample was heated to 80 °C in a convection oven, leading to full recovery of its original shape. This loading-recovery process was repeated a second time to analyze whether the mechanical properties of the sample were compromised from the first stretch. Next, a custom-made double edge notch punch (see the Supporting Information, Figure S4) was used to create two collinear, gauge-centered edge-cracks that were 0.5 mm long on each side of the dogbone neck. The notched sample was then stretched to a displacement of 5 mm (corresponding to a strain of 30%) to macroscopically and controllably damage the sample and propagate the crack extensively, but leave a central ligament. The whole process was followed by real time imaging using a Zeiss Discovery V8 stereo microscope with a QIMAGING (QICAM FAST1394) CCD camera. The damaged sample was then "self-healed" (or thermally mended) by heating to 80 °C and holding isothermally for 10 min, during which time the SM mechanism was triggered and assisted in crack closure by the n-PCL, while the SH mechanism allowed for crack

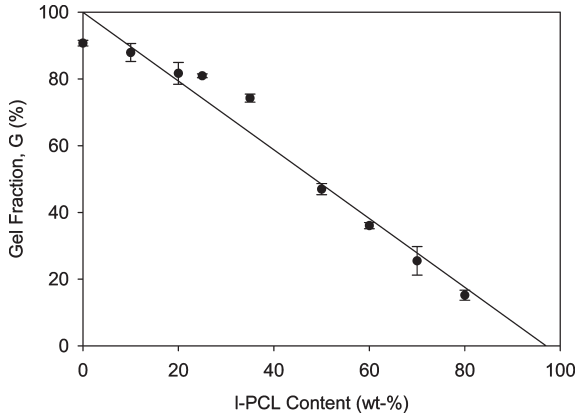

Figure 1. Dependence of the n-PCL:l-PCL gel fraction, $G(\%)$, by $CHCl_3$ extraction of all compositions tested as a function of l-PCL wt % content and taken for an average of three samples. The line represents linear regression of the data, revealing small deviation of the expected extraction of all l-PCL.

rebonding. This healed specimen was then tested with the same tensile deformation without renotching to measure SH efficiency, which was defined as

$$\eta(\%) = \frac{P^{max}_{healed}}{P^{max}_{virgin}} \times 100 \qquad (2)$$

where the virgin (P^{max}_{healed}) and healed (P^{max}_{virgin}) peak loads were obtained from the force vs displacement curves recorded for sample's virgin and healed state when stretched on the Linkam tensile stage. After this test, if the sample had not fractured in two it was thermally treated and tested yet one more time, labeled "After 2nd Thermal Mending", again without additional notching.

RESULTS AND DISCUSSION

Preparation and Thermal Analysis of l-PCL:n-PCL Networks. Gel fraction (GF) experiments were conducted to evaluate the network content of the linear/network blends and the results are shown in Figure 1. To do this, nine compositions with varying l-PCL and n-PCL wt % content were prepared by solvent blending followed by a UV-initiated thiol−ene reaction photopolymerization. Next, GF measurements were conducted by chloroform extraction, noting that l-PCL is soluble in this solvent. If all the PCL diacrylate molecules reacted with the thiol groups during photopolymerization, the GF would show a linear relationship with l-PCL wt % (Figure 1). We anticipated complete extraction of the linear component from the network. All samples were visually turbid prior to solvent swelling but transformed into a transparent state after swelling had stabilized at 24 h. The samples all remained intact during swelling, but were significantly enlarged because of the solvent swelling the sample. A thin, white layer of unreacted PCL diacrylate and/or l-PCL was evident in the extraction jar where the GF experiment took place once the solvent evaporated. Gel fractions obtained (shown in Table S3 in the Supporting Information) ranged from 90.7% for l-PCL_0:n-PCL_{100} to 15.2% for l-PCL_{20}:n-PCL_{80}. The GF values of the remaining compositions lay within the range stated above. Our GF show reasonable agreement with our expectation that only l-PCL would be extracted and that small (<10%) extraction of n-PCL components occurred because of network imperfections.

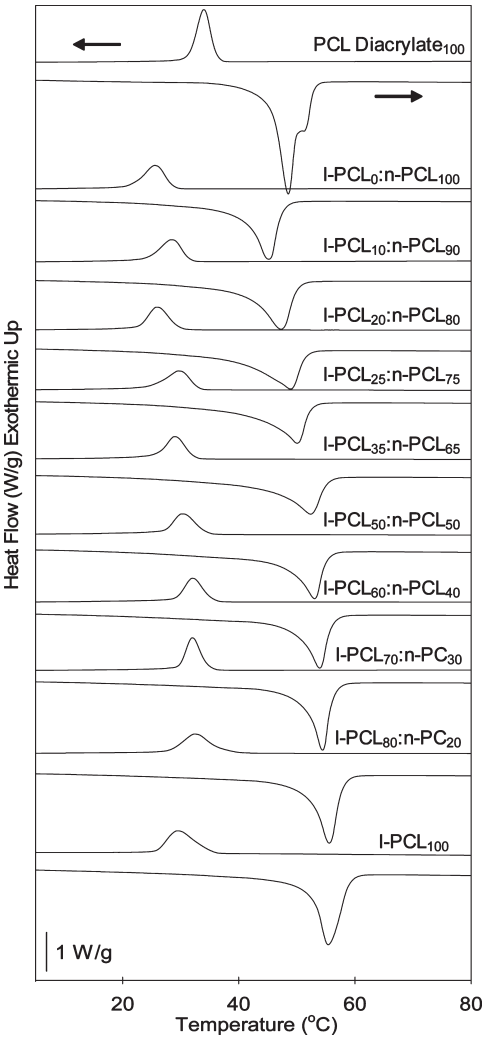

Figure 2. Representative heating and cooling DSC traces showing the T_m and T_c of all compositions tested. The first and second heating were conducted at 10.0 °C/min to 120 °C with a cooling rate at 3.0 °C/min to −90 °C.

DSC experiments were conducted to understand the thermal transitions of each composition as they relate to the thermomechanical properties, which will be presented below. First cooling and second heating DSC traces are shown in Figure 2 for all linear/network compositions, as well as the PCL diacrylate$_{100}$ and l-PCL_{100} samples for comparison. Although all compositions tested show similar melting and crystallization temperatures, a clear trend in T_m is evident: as the percentage of l-PCL increases, the melting point increases in a manner approaching pure linear PCL. Further, it is visually evident that intermediate compositions feature broader melting transitions than the limiting cases. These trends are discussed quantitatively in what follows. The average of three traces of T_m, T_c, ΔH_m, and ΔH_c are shown in Table S2 in the Supporting Information.

The trends of T_m, T_c, ΔH_m, and ΔH_c as a function of l-PCL wt % are shown in Figure 3. T_m, T_c, ΔH_m, and ΔH_c values showed an overall increasing trend with the increase of l-PCL wt % content among the compositions. This phenomenon is attributed not only to a higher l-PCL M_w compared to the PCL diacrylate M_w, but may also due to the increase in l-PCL lamellar thickness, which require more energy to melt. This latter

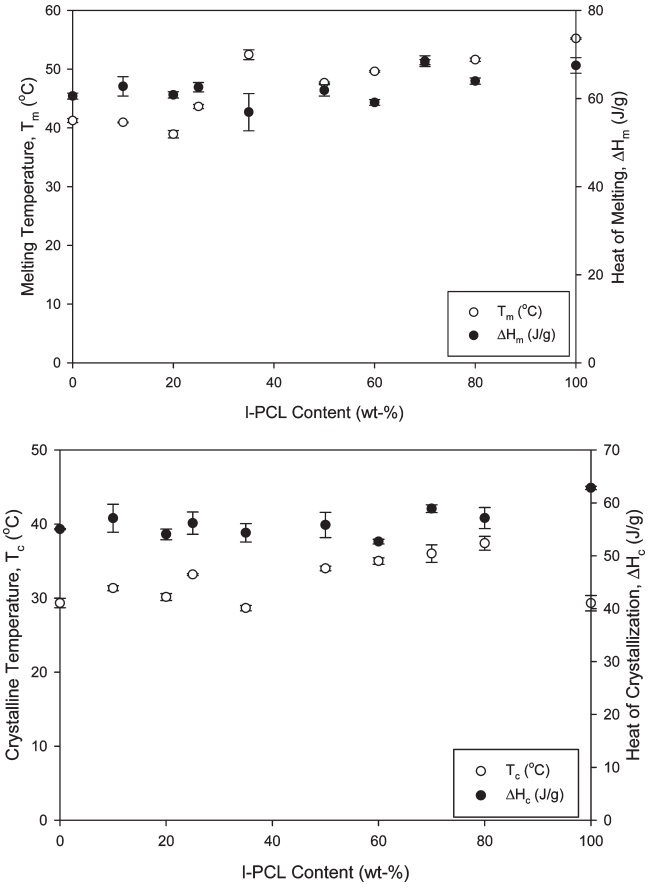

Figure 3. Trends of transition temperatures and latent heats for the blends: (a) T_m and ΔH_m, (b) T_c and ΔH_c as a function of l-PCL wt % content showing average values from three samples tested for each composition.

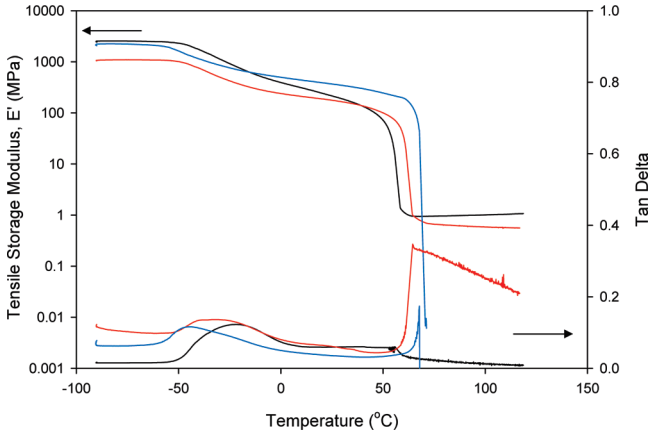

Figure 4. Tensile storage modulus as a function of temperature for l-PCL_0:n-PCL_{100} (black), l-PCL_{50}:n-PCL_{50} (red), and l-PCL_{100} (blue). The first heating was conducted at 3.00 °C/min to 90 °C, followed by cooling at 3.00 °C/min to −90 °C and the second heating at 3.00 °C/min to 120 °C. The first heating for the l-PCL_{100} sample was done at 3 °C/min to 50 °C, cooling at 3 °C/min to −90 °C, and the second heating at 3 °C/min to 70 °C. Second heating data are shown for all samples. The tan delta curves are also shown, indicating the ratio of the viscous to elastic contribution of the samples tested with a peak at T_g and a dramatic rise at T_m.

postulation is beyond the scope of the present paper, but bears future investigation.

Dynamic Mechanical Analysis of l-PCL:n-PCL Networks. Thermomechanical testing was conducted to understand how the linear viscoelastic properties of the compositions depended on temperature. This set of testing is important to provide context for subsequent characterization of SM cycles. Tensile storage modulus (E') and tan(δ) as a functions of temperature are reported for the following compositions: l-PCL_0:n-PCL_{100}, l-PCL_{50}:n-PCL_{50}, and l-PCL_{100} (Figure 4). The remaining compositions showed similar behavior and are shown in Figure S5 in the Supporting Information. All samples showed two distinct thermal transitions: the glass transitions (T_g) were evident at approximately −50 °C where the initiation of polymer chain mobility occurred, while the melting transitions (T_m) appeared at near 55 °C. The tensile storage modulus was at or above 1000 MPa below T_g, beyond which it decreased gradually to ∼100 MPa and then sharply to ca. 1 MPa beyond T_m for cross-linking samples or below a measurable level for l-PCL_{100}. This drop in modulus above T_m was to a modulus plateau indicative of the cross-link density of the entropic rubbery state. As self-healing will be shown to depend on shape memory for crack closure, this rubber elastic state is critical to successful healing of cracks. Although the tensile storage modulus at 25 °C was largely insensitive to the l-PCL content in the blends, the modulus at 80 °C did decrease markedly with l-PCL wt % content, because of dilution of the cross-linked network. These trends with composition are shown in the Supporting Information (Figure S6).

Shape Memory (SM) Characterization. All of the blends containing some portion of n-PCL exhibited shape memory, owing to the fixing of strain by PCL crystallization and recovery of strain by rubber elasticity. Similar reports of shape memory in PCL networks have appeared in the literature.[3,7] Here, we exploit a shape memory cycle (SMC) for semicrystalline polymers that we term as Reversible Plasticity Shape Memory (RPSM).[32] RPSM is a SMC where the material can be deformed to a temporary state *below* a critical temperature (here, T_m), thereby achieving high levels of strain through both elastic (preyield) and plastic (postyield) deformation regions. Remarkably, heating above T_m leads to recovery of both pre- and postyield strain under the action of unimpeded rubber elasticity, thus the term "reversible plasticity." Representative RPSM cycles are shown in Figure 5 for two compositions (discussed further below). In contrast, conventional SMCs involve deformation above T_g or T_m in order to reach a desired temporal strain where only the elastic deformation region is evident and recovered.[1,5−7,28] RPSM assists in the SH process, as it promotes contact between the cracked surfaces formed during damage.

As shown in Figure 5, each sample was stretched at RT to ∼200% strain to achieve temporary deformation (step 1−2). During this deformation step, the PCL crystalline lamellae and constituent polymer chains are envisioned to deform with alignment parallel to the loading axis, experiencing cold draw beyond the yield point. This is evident in the dashed green curve representing a projection of the data on the stress−strain plane for the l-PCL_{50}:n-PCL_{50} composition. The sample was then fixed at this strain to allow for any stress relaxation of the material. The strain was released to observe the initial elastic shape recovery (Figure 5, step 2−3), and the sample then heated to 80 °C to trigger quite complete shape recovery (Figure 5, step 3−4). Finally, the sample was cooled to RT to complete the cycle (Figure 5, step 4−5). All blend compositions were tested in such

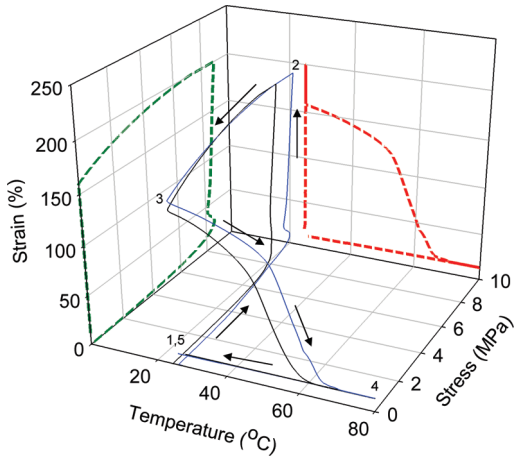

Figure 5. Reversible plasticity shape memory cycle (RPSM) of l-PCL$_0$:n-PCL$_{100}$ (black) and l-PCL$_{50}$:n-PCL$_{50}$ (blue) compositions where each sample was stretched to a strain of 200% at RT and recovered at 80 °C. Strain vs temperature curve (red) and stress vs strain curve (green) are also shown for the l-PCL$_{50}$:n-PCL$_{50}$ composition.

Table 1. Shape Memory Characteristics As a Function of l-PCL wt %

l-PCL$_{wt\ \%}$:n-PCL$_{wt\ \%}$	ε_m (%)	ε_u (%)	ε_p (%)	R_f (%)	R_r (%)
(0:100)	200	151.9	12.7	75.9	91.6
(10:90)	200	150.3	17.3	75.1	88.5
(20:80)	200	148.3	25.9	74.1	82.6
(25:75)	200	156.0	15.4	78.0	90.1
(35:65)	200	150.7	13.0	75.4	91.4
(50:50)	200	160.1	11.6	80.1	92.7
(60:40)	200	158.2	14.4	79.1	90.9
(70:30)	200	161.8	22.0	80.9	86.5
(80:20)	200	161.7	50.0	80.8	69.1

a manner and showed behavior similar to that shown in Figure 5 (results are shown in the Supporting Information (Figure S7)). This demonstrates that RPSM can be achieved for the semicrystalline thermoset/thermoplastic SMASH systems. We anticipated that this behavior would assist in the self-healing process by aiding in the crack closure step.

The shape memory fixing and recovery figures-of-merit, R_f and R_r, calculated from the RPSM cycles for all samples tested are reported in Table 1. All compositions achieved a temporary deformation of 200% strain before unloading (ε_m) with a strain ranging from 148.3 to 161.8% after unloading (ε_u) and a residual strain ranging from 11.6% to 50% (ε_r) after shape recovery. The residual strain is quite small compared to the high temporal deformation that each sample achieved prior to shape recovery. Quantitatively, R_f increased from 74.1 to 80.9% as l-PCL content increased, whereas R_r decreased from 92.7 to 69.1% as l-PCL content increased. (see Figure S8 for a R_f and R_r bar graph). The high recovery ratios observed in the SM cycles will increase the probability of SH, as this recovery will assist in closing cracks found in the bulk of the material.

Self-Healing (SH) Characterization. Having demonstrated shape memory behavior conducive to requisite crack-closure, we conducted SH experiments (described in the Experimental Section) in order to test for the degree of mechanical healing as a function of l-PCL content (wt %). In particular, SH efficiency was determined by comparing the peak loads achieved during tensile testing of the virgin and healed states of samples damaged with the DDEN-T geometry (see Figure S4 in the Supporting Information). Each sample in its virgin, damaged, and healed states was stretched above its yield point then thermally treated to recover and heal by l-PCL diffusion. SH experiments revealed that samples containing 25 wt % or more of l-PCL completely healed after the first thermal treatment with no evidence of crack reopening (see Figure S9 in the Supporting Information for all nine compositions tested). Most importantly, these samples show that the initial cracks made prior to stretching and the propagated crack created while stretching the sample have completely healed when heated above the T_m. A representative example is shown in Figure 6a for the l-PCL$_{50}$:n-PCL$_{50}$ composition. Data reported in Figures 6a and 7 are for individual specimens that are tested first without damage (virgin first stretch, virgin second stretch) and then following damage (notched) and repeated mending cycles (After first, second, and third thermal mending). Such testing was repeated in triplicate for all compositions. The peak loads corresponding to the initial deformation, damaged, and healed states of this composition were 26.6 N, 24.3 N, and 27.5 N, respectively. The data recorded from the force vs displacement curves were compiled to obtain the average peak loads as a function of l-PCL wt % obtained after the first, second, and third thermal mending steps for all compositions tested (see Figure S10 in the Supporting Information). It is noted that loads and displacements are plotted instead of stresses and strains, owing to the geometric complexity making the latter difficult to estimate accurately. Furthermore, there are variable length "toe-regions" (compliant regions near the origin) indicative of variable sample slack incurred during sample loading — these regions should be ignored. Nevertheless, the average tensile yield stress as a function of l-PCL wt % for the sample's virgin and healed state were calculated and shown in Figure S11 in the Supporting Infomration. Importantly, loads were compared for SH efficiency only for individual samples so that internal consistency is assured. We observed that the peak loads associated with the initial deformations were consistently higher than the peak loads of samples in the damaged state. However, heating the samples resulted in remarkable healing. In their healed state, the samples exhibited mechanical properties comparable to the virgin state when comparing the peak loads before damage and after healing. During the second and third thermal mending steps, there was no indication of crack reopening, but rather a necking effect that is apparent in ductile thermoplastic materials.[33]

Figure 6b shows the force vs displacement curve for a notched l-PCL$_{50}$:n-PCL$_{50}$ sample that was stretched in its damaged state, showing stereo micrographs of the sample in its prestretched, initial crack opening, crack transition, and partial crack propagated state. We observe in Figure 6b the sample after damage and before uniaxial stretching followed by the sample's yield point of initial crack opening (transition from the elastic to plastic deformation state). This state is then followed by initial crack growth (crack transition) and finally partially cracked state where the hourglass geometry is evident. This characteristic curve showing crack propagation gives way to the same form as the undamaged sample (yield, followed by cold-drawing), as seen by comparing the solid blue curved (damaged) with the solid red curve (healed) of Figure 6a. This shows indirectly that the collinear cracks have been closed and rebonded successfully by the SMASH mending process. More directly, Figure 6c shows

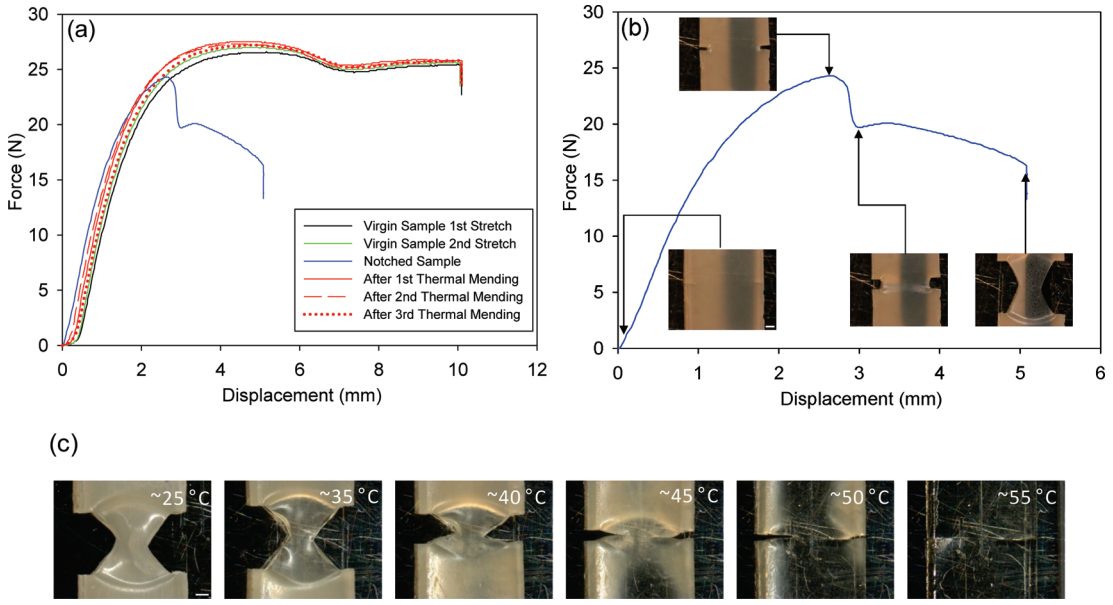

Figure 6. (a) Force vs displacement curves for the virgin, damaged and healed state of a l-PCL_{50}:n-PCL_{50} sample. (b) Notched l-PCL_{50}:n-PCL_{50} sample showing stereo micrographs of deformation and crack growth clamped in the Linkam tensile stage (scale bar: 500 μm). (c) Snapshots of crack closure and crack rebonding when the sample was unclamped from the Linkam tensile stage and heated to the temperatures shown above (stereo micrographs scale bar: 500 μm).

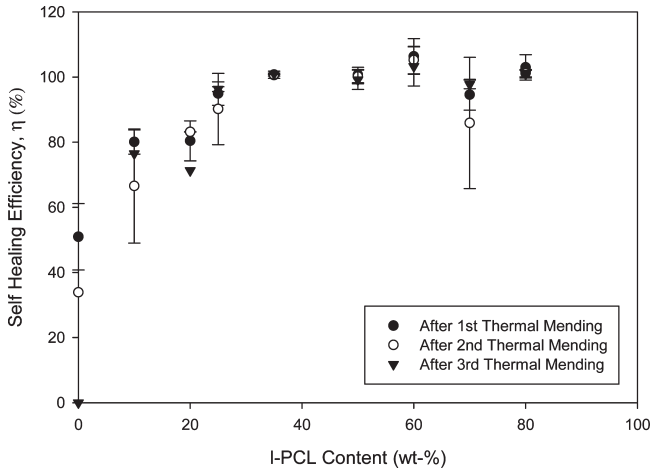

Figure 7. Dependence of self-healing efficiency on l-PCL wt %. The average of three samples tested for SH efficiency for each l-PCL content following first, second, and third thermal mending treatments are shown.

the thermally stimulated closure of the two collinear cracks upon heating the l-PCL_{50}:n-PCL_{50} sample above T_m. As the melting point is exceeded, the sample contracts axially, closing the cracks. At the same time, the samples become optically transparent, indicating that melting of both n-PCL and l-PCL is associated with healing, as expected.

Self-Healing Efficiency Analysis. Figure 7 shows the SH efficiency trend for all compositions tested where complete healing is evident with compositions containing 25 wt % of l-PCL and greater. SH efficiency was calculated as a function of l-PCL wt % for the first, second and third thermal mending treatments (Figure 7). In a thorough review paper on self-healing,[11] it was suggested that the ratio of fractured stress or the elongation-at-break for the healed and virgin states of the sample can serve as a measure of the SH efficiency. However, such properties could not be directly applied to the present (SMASH) system, as a complete fracture into two pieces would prohibit the SM mechanism. Instead, crack propagation of the collinear cracks proceeded to the point of partial fracture, yielding a finite ligament[34] located between the two partially propagated cracks. The strain energy stored in the ligament was ostensibly sufficient to drive the shape recovery component of self-healing (Figure 6c).

Figure 7 shows that compositions containing 20 wt % l-PCL and below have only modest SH efficiency for the first thermal mending treatment, with values ranging from ~50−80%. Compositions containing 25 wt % PCL and higher featured 90% or higher SH efficiency after the first thermal mending treatment and sustained this efficiency for the second and third thermal mending treatments for which the initial and propagated crack regions did not reopen. Thus, excellent shape-memory assisted self-healing is achieved when the l-PCL content in the SMASH system is above 25 wt %. As proven prior, the material is capable of not only recovering its elastic and plastic region (see Figure S12 in the Supporting Information) from damage by its SM mechanism, but the material also has the capacity to heal both the initial and propagated region of damage and still sustain its mechanical properties, quite a distinguishable phenomenon. All samples that contained 20 wt % l-PCL or lower showed no evidence of complete healing after the first thermal mending treatment.

DISCUSSION

The crack profile created during crack propagation is an important area to study as this helps explain the fracture mechanics of ductile polymer materials. During the damage step of our self-healing experiments, the hourglass crack profile that formed (Figure 6b) was one that is characteristic for semicrystalline materials. We have also classified the crack profile into three regions on the basis of SEM observations of the healed specimens (Figure 8): (i) initial crack region created by the double edge notch cutting die, the (ii) crack transition region

dx.doi.org/10.1021/am101012c |ACS Appl. Mater. Interfaces 2011, 3, 152–161

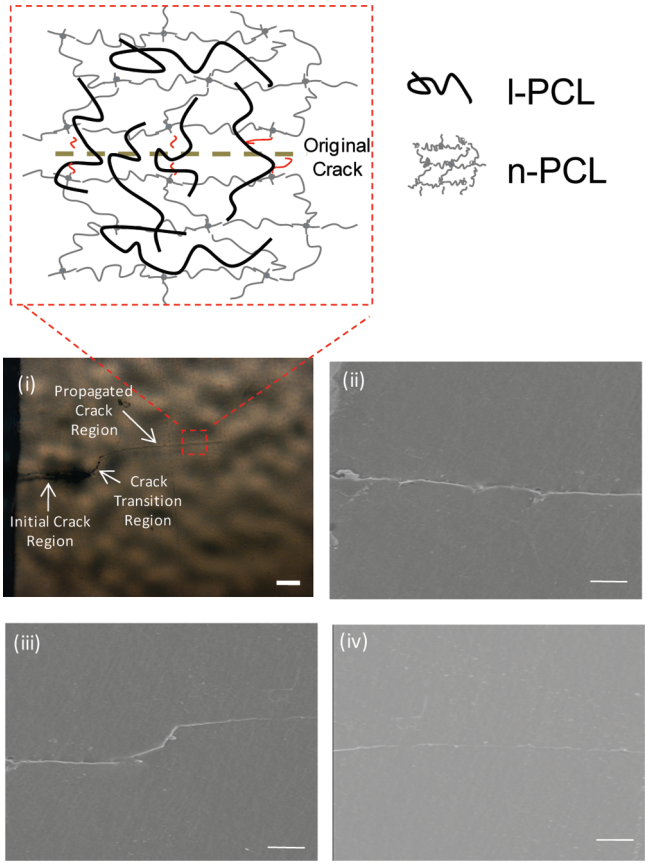

Figure 8. (i) Optical micrograph indicating the three crack regions and an illustration showing schematic of l-PCL chain entanglement in n-PCL. SEM micrographs of healed (ii) initial crack region, (iii) crack transition region, (iv) propagated crack region (scale bars: optical micrograph, 100 μm; SEM, 50 μm).

where the sample reached its yield point and the initiation of crack propagation begins, and (iii) the propagated crack region where new crack surfaces were made. (Additional SEM images of this crack profile (edge views) are given in Figure S12 in the Supporting Information). Figure 8 also includes a schematic of our envisioned l-PCL chain diffusion across the crack surfaces and re-entanglement for SH. This is discussed further below.

The crack profile observed in our experiments has also been observed by Fayolle et al. where they report that the essential work of fracture (EWF) can be used to study ductile fracture under plane stress conditions.[34] (We have not employed this method for toughness measurements, as complete fracture is required.) The load−displacement curves and underlying phenomena of EWF-type analyses can be categorized into two components, the essential work of fracture (EWF) and nonessential work of fracture (non-EWF).[34−36] EWF is defined as the work needed to form new crack surfaces in the process zone, which is also referred to as the ligament region located between the two notches formed, while non-EWF is the work consumed in the outer plastic region. Consequently, the area under the force vs displacement curve (characteristic shape shown in our Figure 6, blue curve) recorded for each fracture test yields the total fracture energy.

Five Stages of Healing. The process of SH within the SMASH material can be explained from the material's SM mechanism and understanding the diffusion and l-PCL chain

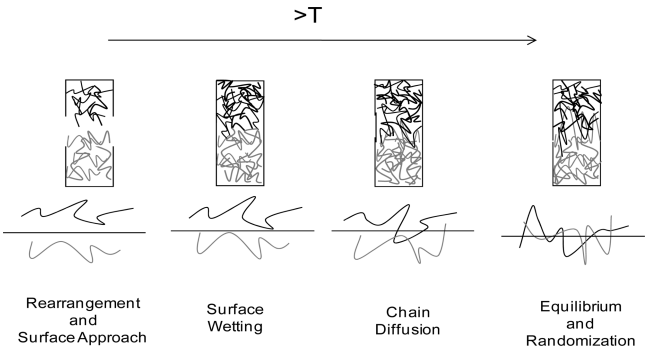

Figure 9. Schematic of five stages of healing (adapted from refs 9 and 28).

entanglement across the site of prior fracture. Considering the l-PCL chains to be capable of diffusion through the n-PCL network, the envisioned five stages of healing are as follows: (1) polymer rearrangement, (2) surface approach, (3) surface wetting, (4) chain diffusion, and (5) equilibrium and randomization (Figure 9).[11,37] After the SMASH material has been damaged at RT, two phenomena occur when the material is heated above T_m: (1) the l-PCL chains start to rearrange as the polymer chains become mobile and the surface tackifies through a population of linear chain ends. (2) The n-PCL transitions from a fixed, strained state of a deformed rubber state, the rubber elasticity gradually overwhelming the stiffness of the diminishing crystalline phases. Thus, the n-PCL-based SM drives crack closure, bringing the crack surfaces into proximity (surface approach). Following this surface approach, l-PCL surface wetting will take place as the two damaged crack surfaces make contact and the initial stage of l-PCL chain diffusion across the crack surfaces occurs. Finally, the system will approach a state of equilibrium as complete l-PCL chain diffusion occurs and chain randomization leads to strengthening re-entanglement. Finally, as the SMASH material is cooled to RT, both the n-PCL and l-PCL components recrystallize, yielding a surface "scar" as evidence of the crack rebonding (Figure 8).

CONCLUSIONS

We have presented a new self-healing polymeric system that combines shape memory and thermoplastic diffusion for crack-closure and rebonding, respectively. Dynamic mechanical analysis revealed that all samples featuring some n-PCL (network) component exist in a rubbery state above T_m, whereas the healing agent, l-PCL_{100}, becomes a viscous liquid above the T_m. A particular type of shape memory, RPSM, was demonstrated, wherein a large deformation of 200% strain at RT was followed by nearly complete recovery upon heating above T_m. Self-healing tests showed that damage imparted in the controlled manner of DDEN-T specimens was well-healed when the samples were heated above T_m. Those samples that contained 25 wt % of l-PCL and higher showed complete healing where only necking occurred in subsequent testing, indicating that the two crack surfaces fully rebonded together due to re-entanglement of the l-PCL adhesive component in the material. Thus, both the initial and propagated cracks are healed during thermal mending. SH efficiency analysis revealed that the mechanical properties for the compositions containing 25 wt % l-PCL and higher showed an efficiency of 95% or higher. We anticipate further studies with this and other SMASH systems exploring

application as self-healing tank-lining bladders, inflated structure membranes, and architectural building envelopes, among others. Heating for such applications could be supplied externally by a maintenance procedure of convection or radiative heating, externally by ambient conditions such as sunlight or aerodynamic heating, or internally by Joule heating.[38] Given the low rubber modulus above T_m, the SMASH article may need to be mechanically supported. Certainly, the heating scheme will be tailored to the demands of particular applications.

■ ASSOCIATED CONTENT

Supporting Information. (1) ^{1}H NMR spectrum of PCL diol(3k). (2) ^{1}H NMR spectrum of PCL diacrylate(3k). (3) TGA curve of l-PCL$_0$:n-PCL$_{100}$. (4) Custom made double edge notch punch. (5) Conventional DMA of all nine compositions tested as a function of temperature. (6) Tensile storage modulus trends for all compositions tested at 25 and 80 °C. (7) Reversible plasticity shape memory cycle (RPSM) for all nine compositions tested. (8) Fixing (R_f) and Recovery (R_r) ratios for all nine compositions tested as a function l-PCL wt % content. (9) Graphs showing deformed, damaged and healed force vs displacement curves for all nine compositions tested. (10) Average peak loads as a function of l-PCL wt % content after each thermal mending treatment. (11) Average tensile yield stress as a function of l-PCL wt % content for each virgin and healed samples tested. (12) Stereo micrographs and SEM images of the elastic and plastic regions of damage. Tables S1 and S2 report PCL diol "n" values and end-capping conversion percentage, respectively. Table S3 of gel fraction (G(%)) average of three samples tested for each compositions. Table S4 showing the average T_m, ΔH_m, T_c, and ΔH_c averages for all compositions tested (PDF). This material is available free of charge via the Internet at http://pubs.acs.org.

■ AUTHOR INFORMATION

Corresponding Author

*E-mail: ptmather@syr.edu. Tel: (315) 443-8760. Fax: (315) 443-9175.

■ ACKNOWLEDGMENT

P.T.M. acknowledges support from AFRL SBIR (Contract FA8651-07-C-0105) and NSF (DMR-0758631). E.D.R. acknowledges support from Syracuse University in the form of a Science, Technology, Engineering and Mathematics (STEM) fellowship. E.D.R. also acknowledges Dr. Kazuki Ishida for his assistance in NMR analysis and Dr. Taekwoong Chung for polymer synthesis assistance.

■ REFERENCES

(1) Mather, P. T.; Luo, X. F.; Rousseau, I. A. *Annu. Rev. Mater. Res.* **2009**, *39*, 445–471.
(2) Rousseau, I. A. *Polym. Eng. Sci.* **2008**, *48*, 2075–2089.
(3) Lendlein, A.; Kelch, S. *Angew. Chem., Int. Ed.* **2002**, *41*, 2034–2057.
(4) Lendlein, A.; Schmidt, A. M.; Schroeter, M.; Langer, R. *J. Polym. Sci., Part A* **2005**, *43*, 1369–1381.
(5) Liu, C.; Qin, H.; Mather, P. T. *J. Mater. Chem.* **2007**, *17*, 1543–1558.
(6) Chung, T.; Romo-Uribe, A.; Mather, P. T. *Macromolecules* **2008**, *41*, 184–192.
(7) Lee, K. M.; Knight, P. T.; Chung, T.; Mather, P. T. *Macromolecules* **2008**, *41*, 4730–4738.
(8) Knight, P. T.; Lee, K. M.; Chung, T.; Mather, P. T. *Macromolecules* **2009**, *42*, 6596–6605.
(9) Lowe, A. B. *Polym. Chem.* **2010**, *1*, 17–36.
(10) Hoyle, C. E.; Bowman, C. N. *Angew. Chem., Int. Ed.* **2010**, *49*, 1540–1573.
(11) Wu, D. Y.; Meure, S.; Solomon, D. *Prog. Polym. Sci.* **2008**, *33*, 479–522.
(12) White, S. R.; Sottos, N. R.; Geubelle, P. H.; Moore, J. S.; Kessler, M. R.; Sriram, S. R.; Brown, E. N.; Viswanathan, S. *Nature* **2001**, *409*, 794–797.
(13) Cosco, S.; Ambrogi, V.; Musto, P.; Carfagna, C. *J. Appl. Polym. Sci.* **2007**, *105*, 1400–1411.
(14) Yuan, L.; Liang, G. Z.; Xie, J. Q.; Li, L.; Guo, J. *Polymer* **2006**, *47*, 5338–5349.
(15) Keller, M. W.; White, S. R.; Sottos, N. R. *Adv. Funct. Mater.* **2007**, *17*, 2399–2404.
(16) Caruso, M. M.; Blaiszik, B. J.; White, S. R.; Sottos, N. R.; Moore, J. S. *Adv. Funct. Mater.* **2008**, *18*, 1898–1904.
(17) Williams, G.; Trask, R.; Bond, I. *Composites, Part A* **2007**, *38*, 1525–1532.
(18) Trask, R. S.; Bond, I. P. *Smart Mater. Struct.* **2006**, *15*, 704–710.
(19) Trask, R. S.; Williams, G. J.; Bond, I. P. *J. R. Soc. Interface* **2007**, *4*, 363–371.
(20) Kirkby, E. L.; Rule, J. D.; Michaud, V. L.; Sottos, N. R.; White, S. R.; Manson, J. A. E. *Adv. Funct. Mater.* **2008**, *18*, 2253–2260.
(21) Kirkby, E. L.; Michaud, V. J.; Manson, J. A. E.; Sottos, N. R.; White, S. R. *Polymer* **2009**, *50*, 5533–5538.
(22) Hayes, S. A.; Jones, F. R.; Marshiya, K.; Zhang, W. *Composites, Part A* **2007**, *38*, 1116–1120.
(23) Meure, S.; Wu, D. Y.; Furman, S. *Acta Mater.* **2009**, *57*, 4312–4320.
(24) Luo, X. F.; Ou, R. Q.; Eberly, D. E.; Singhal, A.; Viratyaporn, W.; Mather, P. T. *ACS Appl. Mater. Interfaces* **2009**, *1*, 612–620.
(25) Chen, X. X.; Dam, M. A.; Ono, K.; Mal, A.; Shen, H. B.; Nutt, S. R.; Sheran, K.; Wudl, F. *Science* **2002**, *295*, 1698–1702.
(26) Chen, X. X.; Wudl, F.; Mal, A. K.; Shen, H. B.; Nutt, S. R. *Macromolecules* **2003**, *36*, 1802–1807.
(27) Rodriguez, E. D.; Luo, X.; Mather, P. T. *Proc. SPIE* **2009**, *7289*, 728912–728912-5.
(28) Luo, X. F.; Mather, P. T. *Macromolecules* **2009**, *42*, 7251–7253.
(29) Cramer, N. B.; Bowman, C. N. *J. Polym. Sci., Part A: Polym. Chem.* **2001**, *39*, 3311–3319.
(30) Decker, C. *Macromol. Rapid Commun.* **2002**, *23*, 1067–1093.
(31) Chung, T. . *Dissertation*, Case Western Reserve University, Cleveland, OH, 2009.
(32) Koerner, H.; Price, G.; Pearce, N. A.; Alexander, M.; Vaia, R. A. *Nat. Mater.* **2004**, *3*, 115–120.
(33) Maspoch, M. L.; Santana, O. O.; Grando, J.; Ferrer, D.; Martinez, A. B. *Polym. Bull.* **1997**, *39*, 249–255.
(34) Fayolle, B.; Tcharkhtchi, A.; Verdu, J. *Polym. Test.* **2004**, *23*, 939–947.
(35) Karger-Kocsis, J.; Ferrer-Balas, D. *Polym. Bull.* **2001**, *46*, 507–512.
(36) Karger-Kocsis, J.; Barany, T.; Moskala, E. J. *Polymer* **2003**, *44*, 5691–5699.
(37) Wool, R. P.; O'Conner, K. M. *J. Appl. Phys.* **1981**, *52*, 5953–5964.
(38) Luo, X. F.; Mather, P. T. *Soft Matter* **2010**, *6*, 6210–6210.